Available online at www.sciencedirect.com
ScienceDirect
Catalysis Today 137 (2008) 475–482
CATALYSIS TODAY
www.elsevier.com/locate/cattod

Development of functionalized Fe–Al–Cr alloy fibers as innovative catalytic oxidation devices

Paolo Fornasiero [a,*], Tiziano Montini [a], Mauro Graziani [a], Stefano Zilio [b], Marco Succi [b]

[a] *Chemistry Department, Center of Excellence for Nanostructured Materials and INSTM-Trieste Research Unit, University of Trieste, via L. Giorgieri 1, 34127 Trieste, Italy*
[b] *SAES Getters SpA, viale Italia 77, 20020 Lainate (Mi), Italy*

Available online 30 January 2008

Abstract

Catalytic devices play a very important role to drastically reduce the noxious contaminants released by the combustion engines. Common devices consist of functionalized ceramic monoliths; an interesting alternative can be realized with a support material made of a high temperature compatible metal alloy, like FeCrAl. In the present study the FeAlCr fibers used to make a device similar to the ceramic monolith were thermally treated to obtain alumina whiskers, which were homogenously covered with alumina or ceria–zirconia–alumina washcoats. Pt or Pt and Pd have been loaded over the functionalized fibers obtaining an innovative oxidation catalyst. The systems were characterized by BET surface area measurements, hydrogen chemisorption and tested under high space velocity and fast heating run-up cycles, for hydrocarbon and CO conversion and particulate filtration ability. The good catalytic activity after severe aging treatments confirms the possibility of use of these innovative functionalized metallic stacks in air pollution control applications.

Keywords: FeAlCr alloys; CO oxidation; Hydrocarbon oxidation; Particulate matter; Ceria–zirconia

1. Introduction

The increase of the world attention to pollution problems is forcing more stringent environmental legislations to limit the exhaust of dangerous gases from combustion engines into the atmosphere. The adoption of prevention strategies or the development of innovative catalytic technologies able to ensure high and efficient pollution conversion is already or will be mandatory for any kind of vehicles. The adoption of car converters (three way catalysts, TWCs) represents the most successful example of large-scale application of heterogeneous catalysts in environmental protection. However, in order to obtain high conversion efficiency, these catalytic converters need to operate under stoichiometric air to fuel ratio (A/F), increasing the fuel consumption [1]. The concern about oil price has focused the attention of the engine manufacturers to the more efficient lean-burn approach. The significantly higher oxygen concentration in the exhausted gases of lean-burn (1–5%) and diesel (5–15%) engine with respect to gasoline car (0.2–2%) has required the development of new strategies for air pollution control [1–5]. In this respect, the reduction of NO under oxidizing conditions, the combustion of soot at low temperature and the oxidation of high amounts of CO and HCs represent the real challenges. The presence of NO in the exhaust gases has been usefully used to *in situ* produce NO_2, a good soot oxidizer (NOx-aided continuous regeneration trap system). Ceramic monoliths are commonly used as base for the catalyst washcoat in TWCs [1,6]. These systems present many advantages, such as low cost, easy of fabrication, high exposed area and a good adhesion of the catalytic material, but they reach slowly the operative temperature. This is a serious limitation for diesel engines, where the exhaust gasses reach temperatures lower than the ones reached by gasoline engines. Metallic monoliths and laminated systems have been therefore developed to avoid this drawback [7–9]; in fact, they have good thermal conductivity. However, the adhesion of the washcoat is low, resulting in a progressive loss of the catalytic active

* Corresponding author. Tel.: +39 040 558 3973; fax: +39 040 558 3903.
E-mail addresses: pfornasiero@units.it (P. Fornasiero), marco_succi@saes-group.com (M. Succi).

0920-5861/$ – see front matter © 2007 Elsevier B.V. All rights reserved.
doi:10.1016/j.cattod.2007.12.097

materials. Formation of Al_2O_3 whiskers on the surface of a metal foil, as a consequence of a thermal oxidation treatment, has been proposed to enhance the adhesion of the washcoat [8,10–12], even if the preparation methods can still be improved. An innovative metallic stack, made by a network of thin metallic wires functionalized by the deposition of nanocomposite heterogeneous catalysts with a similar approach adopted by Shen et al. on FeCrAl foils [13] is proposed.

2. Experimental

2.1. Functionalization of the metallic stack

Commercial FeCrAl alloy (Fe 70%, Cr 25%, Al 5%) non-sintered fiber (diameter ~22 μm) panels were compressed to obtain a stack with specific weight of about 0.2 g/cm^3 and a porosity of more than 98% in volume. The stack looks like a self-consistent cylinder made by fibers randomly distributed (overall dimensions: diameter 64 mm, height 10 mm). The support was washed in deionized water at about 60 °C for 1 h under sonication. After drying, it was treated at 950 °C in ambient air, to grow a rough layer of α-Al_2O_3. Subsequently, washcoat depositions were performed using either a slurry of γ-Al_2O_3 (sol precursor from Sasol) or a mixture of the γ-Al_2O_3 and $Ce_{0.6}Zr_{0.4}O_2$ (Sigma–Aldrich) (1:1 by weight). After deposition and drying, the washcoat was calcined in static air at 700 °C for 5 h. Starting from the respective nitrates (Zentek), 1 wt.% Pt or 0.5 wt.% Pt and 0.5 wt.% Pd were deposited on the washcoat by ionic exchange. After drying, the active phase was reduced under H_2 at 350 °C. The final metal loading was determined by ICP analysis.

2.2. Catalytic activity measurements

The oxidation of 400 ppm of CO and 600 ppm of C_3H_6 (4% O_2 and N_2 balance) was used to study the catalytic activity of the sample. The low oxygen concentration, 4% was choosen to test the catalyst in the most challenging real condition. A total flow of 8 Nm^3 h^{-1} and a residence time of 0.014 s were used to simulate the severe working condition of a diesel oxidation catalyst. A 316 L stainless steel cylindric reactor with a 64 mm internal diameter was fed by the gaseous mixture pre-heated at the desired temperature. C_3H_6 and O_2 were blended with the other gases after the heater to avoid the C_3H_6 cracking on the surface of the heater elements. A multichannel infrared spectrometer ABB URAS 14 was used to continuously monitor CO_2, CO and light HCs at ppm level. The analyser was calibrated using cryogenic N_2 (as zero gas) and a certified cylinder mixture containing 500 ppm CO, 1030 ppm CO_2, 1000 ppm C_3H_6, 10.1% O_2, N_2 balance made by SIAD (as span gas). The sample temperature was progressively increased with a ramp of 30 °C min^{-1} to characterize the samples, both fresh and after aging.

Two different aging protocols were employed: (i) 100 cycles between room temperature and 650 °C (ramp up 300 °C min^{-1}, 5 min soak) flowing 60 Nm^3 h^{-1} of air through the sample or (ii) in ambient static air at 800 °C, about 40% humidity, for 10 h.

Soot filtration efficiency tests were performed using from 1 to 4 g of Vulcan XC72R carbon dispersed in a flow of 40 Nm^3 h^{-1} of air at room temperature. The flow was forced to pass through the filters of 64 mm of diameter and different heights, depending on the fiber density and geometry. Subsequently, soot combustion experiments were carried out using a flow of 50 Nm^3 h^{-1} of air from room temperature 650 °C (ramp up 300 °C min^{-1}).

2.3. Characterization

BET surface area and H_2 chemisorption were performed on a Micromeritics ASAP 2020 apparatus. Surface areas were measured by Kr physisorption at liquid nitrogen temperature after degassing the samples at 350 °C for 12 h. Before H_2 chemisorption experiments, the samples were pre-reduced in a flow of H_2 (5%)/Ar (35 ml min^{-1}) at 200 °C for 1 h and degassed at 400 °C for 5 h. H_2 chemisorption was performed at low temperature (−90 °C, bath of liquid/solid acetone). Typically, an equilibration time of 10 s was employed. Adsorption at very low pressures (2–20 Torr) was used to reduce the contribution of the formation of Pd hydride. Adsorbed volumes were determined by extrapolation to zero pressure of the linear part of the adsorption isotherm. A chemisorption stoichiometry hydrogen:metal = 1:1 was assumed.

Temperature-programmed reduction (TPR) was performed using 0.1 g of each sample. The samples were purged with Ar at 550 °C for 15 min and cooled to room temperature. H_2 (5%)/Ar was admitted to the reactor and the flow allowed to stabilise for 30 min before increasing the temperature to 1273 K (10 °C min^{-1}). H_2 consumption was monitored using a thermal conductivity detector.

Scanning electron microscope (SEM) images were collected on a Zeiss Stereoscan 420 microscope, using the backscattering detector, in order to point out the presence of heavy elements (such as Pt, Pd, Ce and Zr).

3. Results and discussion

The use of a stack of FeCrAl alloy non-sintered fibers in the engine exhaust after treatment offers the advantage of a high

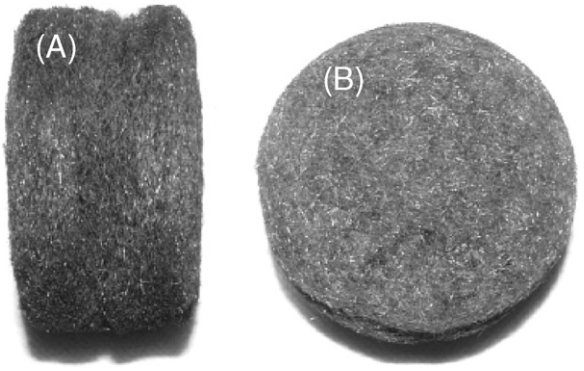

Fig. 1. Representative image of FeCrAl sintered fiber stacks, lateral view (A) and frontal view (B).

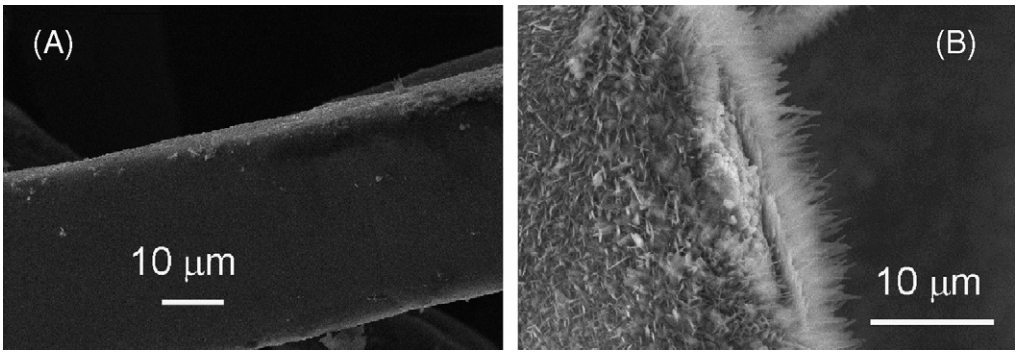

Fig. 2. Representative SEM images of FeCrAl alloy fiber (A) untreated and (B) after thermal treatment in air at 950 °C.

turbulence and a gas–catalyst contact much more efficient than the commercial available ceramic monoliths, where the flow is substantially parallel to the catalytic walls. This would allow using a lower precious metal loading. Furthermore, the high porosity leads to a low-pressure drop, which is mandatory for applications with a high flow rate. Fig. 1 shows the stack used in the experiments to verify the catalytic activity.

Fig. 2 shows that the thermal treatment at 950 °C leads to a significant alumina whiskers formation over the FeCrAl alloy. This layer improves the corrosion resistance and the adhesion of the washcoat [12]. The deposition of the washcoat is a second critical step [14]. In this respect, a slurry deposition appears to be a suitable preparation method. Jia et al. have investigated in details the effects of the slurry properties on coating γ-alumina-based ceramic materials on metal foils [15]. They clearly showed that optimal adhesion of washcoat to FeCrAl foils can be obtained with slurries having pH in the range 4.0–6.0, particle size mainly below 10 μm and a solid content of about 35 wt.%. Furthermore, Jia et al. demonstrated that the presence of ceria–zirconia in the slurry improved the washcoat adhesion to FeCrAl foils and produced a more thermally stable washcoat [15].

More difficult is the realization of a homogeneous deposition of the washcoat on metallic fibers, where the complex geometry can easily lead to the formation of undesirable and thermally unstable aggregates of washcoat particles between the fibers. Fig. 3 indicates that by the proprietary deep coating methodology it was possible to obtain a good fibers coverage with the desirable absence of washcoat particles between the fibers. Even if all the washcoat is normally well distributed on the fibers, some of them have a slightly thicker deposit.

No precious metal particles were discriminated in the fresh samples suggesting high and homogeneous metal dispersion on the surface of the washcoat.

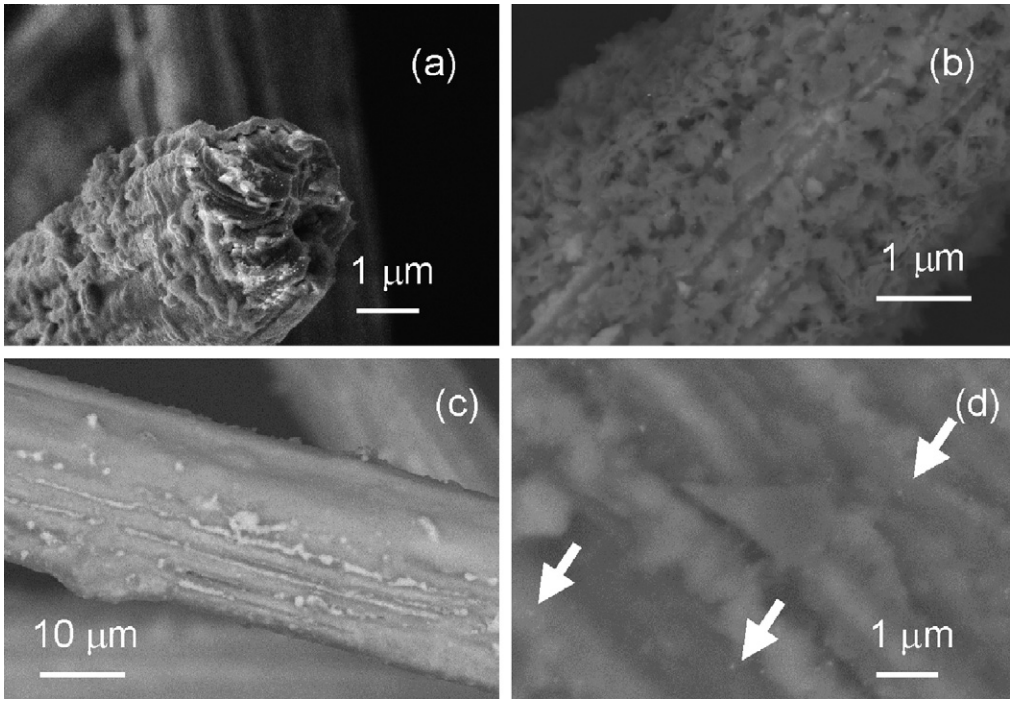

Fig. 3. Representative SEM images of Pt–$Ce_{0.6}Zr_{0.4}O_2$–Al_2O_3/FeCrAl alloy fiber (a–c) fresh and (d) after 100-cycle aging at 650 °C. Arrows highlights examples of Pt clusters (<100 nm).

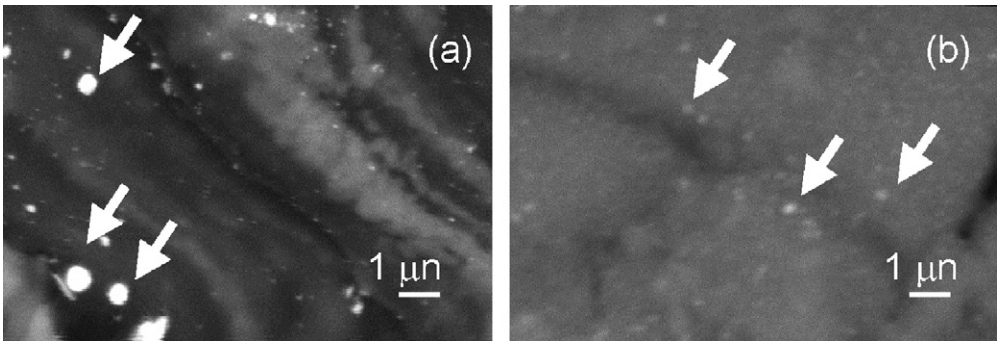

Fig. 4. Examples of SEM images of aged Pt–$Ce_{0.6}Zr_{0.4}O_2$–Al_2O_3/FeCrAl alloy fiber (a) and Pt/Pd–$Ce_{0.6}Zr_{0.4}O_2$–Al_2O_3/FeCrAl alloy fiber (b) after consecutive cycling aging up to 650 °C (10 h) and in static air at 800 °C (10 h). Arrows highlights Pt clusters.

After the severe agings, both under repeated run-up and run-down cycles or in static air at 800 °C, no appreciable macroscopic cracks or other significant washcoat detachments were observed. After the aging cycles up to 650 °C, some small precious metal particles (<100 nm) were detected on all the catalytic phases; the sintered clusters were less abundant on the ceria–zirconia based system, particularly in the case of the Pt/Pd active phase. This is consistent with the ability of the ceria-based oxides to improve metal dispersion and to enhance metal stability [16]. Furthermore, a more severe aging treatment (e.g. 800 °C for 10 h), confirmed the superior thermal stability of the Pt/Pd–$Ce_{0.6}Zr_{0.4}O_2$–Al_2O_3 based system (Fig. 4). In fact, while the aged bimetallic system showed the presence of some metal particles of diameter up to 100 nm, the Pt–$Ce_{0.6}Zr_{0.4}O_2$–Al_2O_3 evidenced also the presence of metal particles with diameter significantly higher (up to 600 nm, Fig. 4).

Table 1 summarizes the composition and the characteristics of the samples. Taking into account the diameter of the metallic wires (~22 μm) and the density of the FeCrAl alloy (7.15 g mL^{-1}), a surface area of ~0.0254 $m^2\,g^{-1}$ can be related to the stack. This value is consistent with the value measured experimentally on the fresh untreated fibers (0.1 $m^2\,g^{-1}$) and it is significantly lower with respect to that measured on the functionalized material (6–10 $m^2\,g^{-1}$). Therefore, the surface area of the materials can be reasonably associated only to the washcoat deposited on the metallic stack. The $Ce_{0.6}Zr_{0.4}O_2$–Al_2O_3 composites present an initial lower surface area with respect to the pure Al_2O_3. After both cyclic aging at 650 °C and static aging at 800 °C, the initial differences are annihilated, consistently with the well-known ability of the rare earth oxides to increase the thermal stability of the alumina. In fact the mutual interaction between the two oxides prevents the transition from γ-Al_2O_3 into α-Al_2O_3 [17].

Hydrogen chemisorption was used to characterize the metal phase. The low adsorption temperature of −90 °C was selected in order to avoid hydrogen spillover onto the ceria-based support [18]. In fact, previous high-resolution transmission electron microscopy (HRTEM) investigations and chemisorption data clearly demonstrated that true Pt dispersion onto ceria–zirconia mixed oxides can be achieved by means of volumetric H_2 chemisorption measurements at low temperature [18]. Furthermore, negligible hydrogen spillover at low temperature was observed in Pt (1%)/$Ce_{0.6}Zr_{0.4}O_2$ (13%)Al_2O_3 nanocomposites [19]. The chemisorption results (Table 2) indicate that all fresh samples have a high apparent metal dispersion and that the cycling aging treatment induces a severe sintering. The concomitant decrease of total surface area (Table 1) suggests that some metal encapsulation can occur as well. The presence of the ceria–zirconia mixed oxide favours the metal dispersion and significantly prevents the loss of the metallic surface area during the aging. The bimetallic systems show the best performances accordingly with the indication that partial Pt/Pd alloys formation can strongly inhibits platinum sintering [20]. However, in the case of the Pd containing system, we cannot exclude that the high Hydrogen/metal ratios are due to the formation of palladium hydrides. Consistently with SEM data, the aging under static conditions further decreases the hydrogen uptake indicating a more severe sintering of the metal phase and/or appreciable encapsulation of the metal phase into the support. This is particular evident in the absence of the ceria–zirconia mixed oxide, accordingly with previous observations [21].

Table 1
Characteristics of the functionalized FeCrAl alloy fiber

Sample	Al_2O_3 (%)[a]	CZ60 (%)[a]	Pt (%)[a]	Pd (%)[a]	BET surface area ($m^2\,g^{-1}$)[b]		
					Fresh	Aged[c]	Aged[d]
Pt–Al_2O_3	10.0	–	0.80	–	93	67	56
Pt–$Ce_{0.6}Zr_{0.4}O_2$–Al_2O_3	5.0	5.0	0.73	–	77	72	59
Pt/Pd–$Ce_{0.6}Zr_{0.4}O_2$–Al_2O_3	5.0	5.0	0.40	0.40	73	70	71

[a] Weight percentage calculated with respect to the final material.
[b] Percentage calculated with respect to the washcoat.
[c] After 100-cycle aging up to 650 °C.
[d] Aged in ambient static air at 800 °C for 10 h, about 40% humidity.

Table 2
Apparent metal dispersion (H/M)[a] and metallic surface area (MSA) obtained from H_2 chemisorption

Sample		Pretreatment	H/M	MSA ($m^2\ g^{-1}$)[d]
$Pt–Al_2O_3$	Fresh	Pre-reduction 200 °C	0.57	1.13
	Aged[b]	Pre-reduction 200 °C	0.19	0.40
	Aged[c]	Pre-reduction 200 °C	0.10	0.20
$Pt–Ce_{0.6}Zr_{0.4}O_2–Al_2O_3$	Fresh	Pre-reduction 200 °C	0.68	1.35
	Aged[b]	Pre-reduction 200 °C	0.35	0.69
	Aged[c]	Pre-reduction 200 °C	0.18	0.38
$Pt/Pd–Ce_{0.6}Zr_{0.4}O_2–Al_2O_3$	Fresh	Pre-reduction 200 °C	0.82	–[e]
	Aged[b]	Pre-reduction 200 °C	0.66	–[e]
	Aged[b]	Pre-reduction 200 °C	0.25	–[e]

[a] Apparent metal dispersion defined as the ratio between the adsorbed hydrogen atoms and the metal atoms, Pt or Pt and Pd (H/M).
[b] After 100 cycle aging up to 650 °C.
[c] Aged in ambient static air at 800 °C for 10 h, about 40% humidity.
[d] Calculated with respect to the washcoat weight.
[e] Not reported to avoid assumption on the relative dispersion of the two metals.

To further investigate the modification of the catalyst under the aging conditions, temperature-programmed reduction experiment were performed (Fig. 5). Presence of complex multipeak reduction profiles indicates the existence of various reducible species. The reduction peaks below 200 °C can be mainly associated with the reduction of Pt or Pd oxides [22], while the intense peak between 500 and 600 °C with the bulk reduction of Ce^{4+} to Ce^{3+} [23]. The reduction peaks observed at intermediate temperature (300–400 °C) could be related to reduction of surface cerium, even thought reduction of surface and bulk cerium can occur concomitantly in ceria–zirconia mixed oxides [23]. The presence of the metal phase, able to activate/dissociate the hydrogen and to spill it over the support can promote support reduction. In this respect the presence of multipeaks could be partially related to the reduction of cerium in different contact with the noble metal phase. Furthermore, presence of multipeaks in this temperature interval could be an indication of heterogeneity in the solid solution [16]. However the adopted synthesis was designed to obtain the formation of a truly solid solution, avoiding significant phase separation. Using conventional techniques for structural characterization, it is not possible to exclude the presence of heterogeneity in the ceria–zirconia mixed oxides, at microdomain level. Finally, the observation of a qualitatively similar pattern in the $Pt–Al_2O_3$ samples suggests the presence of additional contribution, such as reduction of iron oxides or chromium oxides formed during the fibers activation. Notably, the aging procedures progressively suppress the reduction peaks at low temperature, supporting the evidences of metal sintering/encapsulation. In the case of ceria–zirconia containing materials there is also a shift to higher temperature of the Ce^{4+} to Ce^{3+}reduction peak which is consistent with the partial sintering of the support [24].

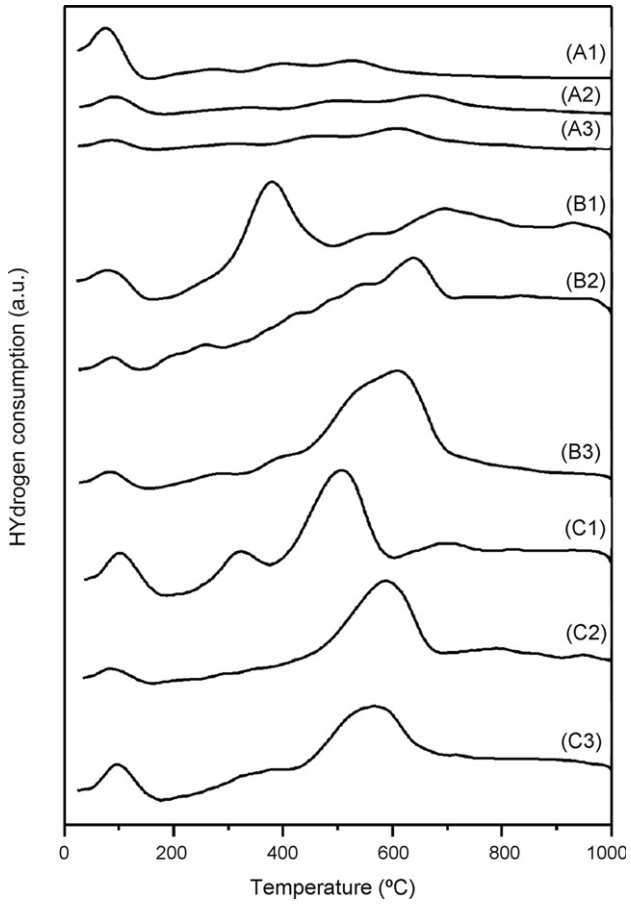

Fig. 5. Temperature-programmed reduction of (A) $Pt–Al_2O_3$, (B) $Pt–Ce_{0.6}Zr_{0.4}O_2–Al_2O_3$ and (C) $Pt/Pd–Ce_{0.6}Zr_{0.4}O_2–Al_2O_3$ over FeCrAl alloy fibers. Trace 1, 2 and 3 indicate fresh samples, samples after 100-cycle aging up to 650 °C and samples after aging under static air at 800 °C for 10 h, respectively.

Fig. 6 shows the catalytic activity with respect to the CO oxidation of the different stacks under simulated exhaust conditions. The activity tests were carried out in the lower range of oxygen concentration to simulate the most unfavorable conditions for the oxidation reactions. Under the same experimental conditions, no CO conversion was obtained on fiber functionalized with only Al_2O_3, while in the presence of $Ce_{0.6}Zr_{0.4}O_2–Al_2O_3$ the maximum CO conversion was 12%, confirming the participation of ceria-based oxides in the oxidation reaction. In the presence of Pt, CO was fully converted below 400 °C. The introduction of the ceria–zirconia mixed oxides enhanced the CO conversion, either improving

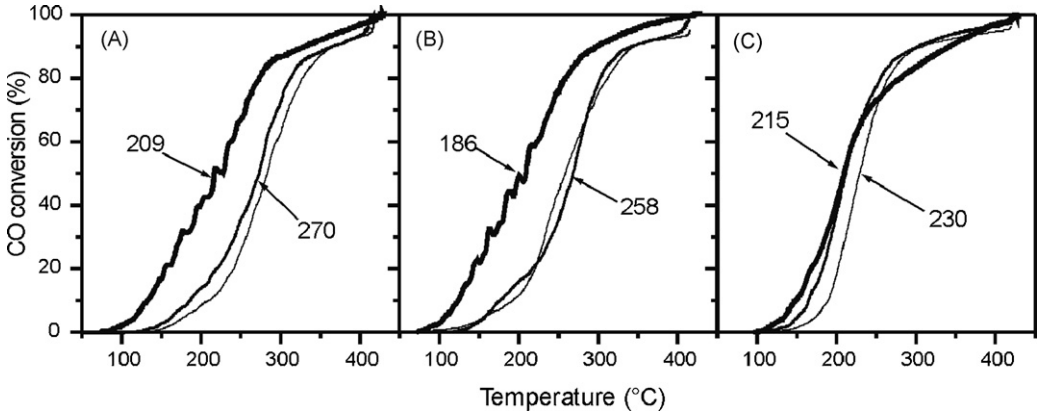

Fig. 6. CO conversion during run-up experiments on (A) Pt–Al_2O_3, (B) Pt–$Ce_{0.6}Zr_{0.4}O_2$–Al_2O_3 and (C) Pt/Pd–$Ce_{0.6}Zr_{0.4}O_2$–Al_2O_3 over FeCrAl alloy fibers. Bold lines indicate fresh samples, thin lines indicate samples after 100-cycle aging up to 650 °C and dashed line indicate samples after aging under static air at 800 °C for 10 h. Light-off temperatures ($T = 50\%$ of conversion) are indicated.

the metal dispersion (Table 2) or involving its reactive lattice oxygen (see above experiment). The aging treatment induced a deactivation of the pure Pt-based catalyst, while it marginally affected the bimetallic Pt/Pd system.

The three fresh systems showed comparable C_3H_6 conversion efficiency (Fig. 7). The cycling aging up to 650 °C led to an appreciable deactivation of the Pt–Al_2O_3 system, to a minor deactivation of the Pt–$Ce_{0.6}Zr_{0.4}O_2$–Al_2O_3 while it did not deactivate the Pt/Pd–$Ce_{0.6}Zr_{0.4}O_2$–Al_2O_3 system. In this latter case, a small improvement in the catalytic activity was observed, which could be associated with some Pd reoxidation, and to a minor contribution due to the formation of an alloy with Pt [20]. Notably, hydrocarbon combustion, especially CH_4, has been the subject of intense studies in the last decade with the aim of correlating catalytic behaviour with the dynamic of Pd–PdO conversion [25]. It has long been recognized that the active phase is palladium oxide [26,27]. It has been shown that cerium oxide is a very effective promoter for Pd reoxidation [28,29]. Indeed, our oxidative aging treatment up to 650 °C can influence the equilibrium between PdO and Pd metal favouring the formation of more reactive palladium species. The aging treatment in static air at 800 °C led to an appreciable deactivation of the C_3H_6 combustion ability for the Pt-based catalyst, while the optimized bimetallic system is less influenced in the C_3H_6 combustion activity.

While the single stack of Pt/Pd–$Ce_{0.6}Zr_{0.4}O_2$–Al_2O_3 functionalized FeCrAl alloy fiber showed good and stable CO and C_3H_6 oxidation ability, its geometry was optimized for catalytic support and not for soot filtration. Nevertheless, a total soot filtration efficiency of about 12% was obtained. Excellent soot filtration efficiencies, even under very high flow rates, were obtained by specifically modulating the overall stack thickness and the type of fibers as shown in Table 3.

During fast run-up experiments (300 °C min^{-1}), all filters loaded with a few grams of synthetic soot showed comparable soot combustion temperature (around 600 °C). Significantly, the presence of a catalyst avoided the CO evolution, which was totally absent in the case of the optimized Pt/Pd–$Ce_{0.6}Zr_{0.4}O_2$–Al_2O_3 functionalized FeCrAl system. The good selectivity toward CO_2 formation and the washcoat adhesion are maintained over many repeated regeneration cycles. By applying a step regeneration process (Fig. 8) it was possible

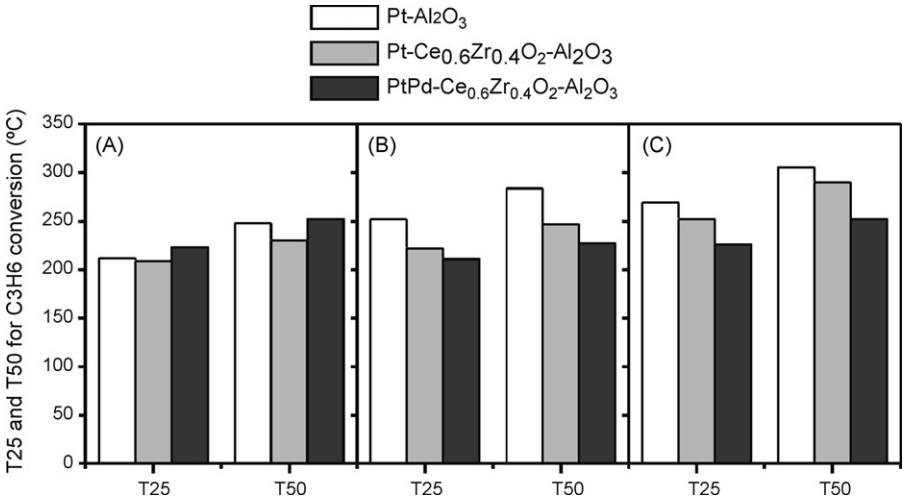

Fig. 7. T25 (temperature corresponding to 25% C_3H_6 conversion) and T50 (temperature corresponding to 50% C_3H_6 conversion) on different stacks. (A) Fresh samples and (B) after 100-cycle aging up to 650 °C and (C) after aging in static air at 800 °C.

Table 3
Examples of synthetic soot filtration efficiency of different fiber stacks

Sample #	Stack thickness (mm)	Type of fiber	Filtration efficiency (%)
1	10	Small fiber diameter	32
2	10	Large fiber diameter	17
3	64	Mixed fiber diameters	89
4	82	Mixed fiber diameters	98

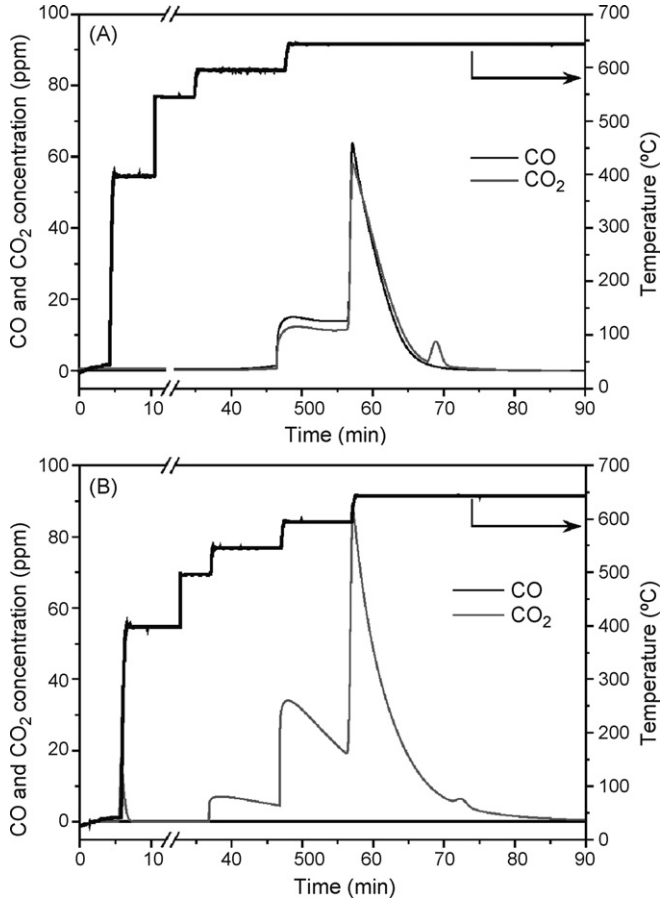

Fig. 8. Regeneration step after loading synthetic soot on (A) FeCrAl alloy fibers and (B) on Pt/Pd–$Ce_{0.6}Zr_{0.4}O_2$–Al_2O_3 over FeCrAl alloy fibers.

to appreciate that the presence of the Pt/Pd–$Ce_{0.6}Zr_{0.4}O_2$–Al_2O_3 catalyst can partially contribute to decrease the temperature and the time of the soot combustion. Notice that the synthetic soot regeneration was performed in ambient air due to experimental system set up. During regeneration in real conditions further improvements of the control of particulate emissions are expected in presence of the catalyst, due to the *in situ* production of NO_2. The oxidation of NO to NO_2 is mandatory not only to oxidize the soot at low temperatures, but also for the NOx adsorption in lean NOx traps.

Finally, SEM analyses showed that an accelerated aging test, consisting in depositing a few grams of ash (5% Fe_2O_3 and 95% lubricant oil) on the stack of fibers before heating them at 900 °C for 7 h in flow of air (40% humidity), does not appreciable modify both the washcoat and the metallic fibers. This confirms the applicability of these materials under the severe real conditions encountered in diesel engine.

4. Conclusions

Metallic fibers have been investigated as alternative substrate to ceramic monoliths in pollution control applications. Good and stable adhesion of ceramic washcoats can be obtained by preforming alumina whiskers on the surface of metallic FeCrAl fibers. Pt or Pt and Pd have been highly dispersed on the washcoat, leading to good oxidation catalysts for CO, hydrocarbon and particulate. Presence of ceria–zirconia mixed oxides proved to have positive influence on metal dispersion and on the oxidation activity. Bimetallic Pt/Pd onto $Ce_{0.6}Zr_{0.4}O_2$–Al_2O_3 washcoat is an optimized combination in terms of activity and thermal stability. The design of geometry of the stack of functionalized fibers is a key point for obtaining good particulate filtration ability. These nanocomposite systems can contribute to control diesel particulate emissions.

The present work highlights the potentiality of functionalized FeCrAl stack of fibers for the treatment of the gas exhausted by combustion engines where high space velocities are required.

Acknowledgements

University of Trieste, CENMAT, INSTM, FISR2002 ‘‘Nanosistemi inorganici ed ibridi per lo sviluppo e l’innovazione di celle a combustibile’’, are gratefully acknowledged for financial support.

References

[1] J. Kaspar, P. Fornasiero, N. Hickey, Catal. Today 77 (2003) 419.
[2] P. Ciambelli, V. Palma, P. Russo, S. Vaccaro, Stud. Surf. Sci. Catal. 116 (1998) 635.
[3] P. Ciambelli, V. Palma, P. Russo, S. Vaccaro, Catal. Today 75 (2002) 471.
[4] R. Burch, J.P. Breen, F.C. Meunier, Appl. Catal. B-Environ. 39 (2002) 283.
[5] R. Burch, P. Fornasiero, B.W.L. Southward, Chem. Commun. (1998) 739.
[6] S. Irandoust, B. Andersson, Catal. Rev.-Sci. Eng. 30 (1988) 341.
[7] E. Tronconi, G. Groppi, Chem. Eng. Sci. 55 (2000) 6021.
[8] J.G. McCarty, M. Gusman, D.M. Lowe, D.L. Hildenbrand, K.N. Lau, Catal. Today 47 (1999) 5.
[9] J. Camra, E. Bielańska, A. Bernasik, K. Kowalski, M. Zimowska, A. Białas, M. Najbar, Catal. Today 105 (2005) 629.
[10] L.R. Chapman, US Patent (1982) 4318828.
[11] L.R. Chapman, C.W. Vigor, J.F. Watton, US Patent (1982) 4331631.
[12] M. Ferrandon, M. Berg, E. Bjornbom, Catal. Today 53 (1999) 647.
[13] M.Q. Shen, L.W. Jia, W.L. Zhou, J. Wang, Y. Huang, Bul. Mater. Sci. 29 (2006) 73.
[14] V. Meille, Appl. Catal. A: Gen. 315 (2006) 1.
[15] L. Jia, M. Shen, J. Wang, Surf. Coatings Technol. 201 (2007) 7159.
[16] J. Kaspar, P. Fornasiero, M. Graziani, Catal. Today 50 (1999) 285.
[17] R. Di Monte, P. Fornasiero, S. Desinan, J. Kaspar, Chem. Mater. 16 (2004) 4273.
[18] J.M. Gatica, R.T. Baker, P. Fornasiero, S. Bernal, J. Kaspar, J. Phys. Chem. B 105 (2001) 1191.
[19] P. Fornasiero, J. Kaspar, T. Montini, M. Graziani, V. Dal Santo, R. Psaro, S. Recchia, J. Mol. Catal. A-Chem. 204 (2003) 683.
[20] A. Morlang, U. Neuhausen, K.V. Klementiev, F.W. Schütze, G. Miehe, H. Fuess, E.S. Lox, Appl. Catal. B: Environ. 60 (2005) 191.

[21] G. Vlaic, P. Fornasiero, G. Martra, E. Fonda, J. Kaspar, L. Marchese, E. Tomat, S. Coluccia, M. Graziani, J. Catal. 190 (2000) 182.
[22] P. Fornasiero, J. Kaspar, V. Sergo, M. Graziani, J. Catal. 182 (1999) 56.
[23] G. Balducci, P. Fornasiero, R. Di Monte, J. Kaspar, S. Meriani, M. Graziani, Catal. Lett. 33 (1995) 193.
[24] P. Fornasiero, T. Montini, M. Graziani, J. Kaspar, A.B. Hungria, A. Martinez-Arias, J.C. Conesa, Phys. Chem. Chem. Phys. 4 (2002) 149.
[25] D. Ciuparu, M.R. Lyubovsky, E. Altman, L.D. Pfefferle, A. Datye, Catal. Rev.-Sci. Eng. 44 (2002) 593.
[26] R. Burch, F.J. Urbano, Appl. Catal. A-Gen. 124 (1995) 121.
[27] P. Forzatti, Catal. Today 83 (2003) 3.
[28] P.O. Thevenin, A. Alcalde, L.J. Pettersson, S.G. Jaras, J.L.G. Fierro, J. Catal. 215 (2003) 78.
[29] S. Colussi, A. Trovarelli, G. Groppi, J. Llorca, Catal. Commun. 8 (2007) 1263.